IDRILL – AN INSTRUMENTED DRILL FOR LUNAR PROSPECTING

T. Tattusch [(1)], J. Biswas [(2)], S. Sheridan[(3)], M. Reganaz [(1)], P. Bruno [(1)], D. Felbach [(1)], C. Gscheidle [(2)], A. Morse[(3)], S. Netter [(1)], I. Pacelli [(1)], A. Palermo [(1)], G. Preißler [(1)], R. Schöggl [(1)], H. Sargeant[(3)], C. Bergemann [(1)], S. Senese [(1)], A. J. Ball [(4)], P. Reiss [(4)]

[(1)] OHB System AG, Manfred-Fuchs-Str. 1, D-82234 Weßling, Germany
Phone: +49 8153 4002 196, email: tim.tattusch@ohb.de
[(2)] Technische Universität München, Institute of Astronautics, Boltzmannstraße 15, 85748 Garching, Germany
Phone: +49 89 289 16018, email: j.biswas@tum.de
[(3)] The Open University, The Robert Hooke Building, Walton Hall, Milton Keynes, MK7 6AA, United Kingdom
Phone: +44 1908 659519, email: simon.sheridan@open.ac.uk
[(4)] European Space research and TEchnology Centre (ESTEC), Keplerlaan 1, PO Box 299, 2200 AG Noordwijk, The Netherlands, Andrew.Ball@esa.int

ABSTRACT

This paper addresses the status of a possible payload instrument for near-term lunar surface mission opportunities, being an instrumented drill for volatiles detection and characterization in the lunar regolith. Extraction of lunar volatiles is becoming increasingly important as they might prove to be a valuable resource for human surface operations or the in-situ production of consumables. iDRILL has been pre-developed since 2016 by OHB System AG, Technical University of Munich (TUM) and The Open University (OU), to the level of an end-to-end prototype, developed for and tested under simulated lunar conditions.
This paper addresses the current status of the project. The scientific background and its impact on design trades is presented, followed by a discussion of the mechanisms and key scientific elements. Furthermore, results of the functional and performance tests are discussed providing an insight into the capabilities and limitations of the instrument.

1 iDRILL INSTRUMENT

The instrumented drill (iDRILL) is a versatile payload instrument for near-term lunar landing mission opportunities, for detection and characterization of lunar volatiles in the shallow subsurface
In contrast to common oven based concepts, the iDRILL instrument does not require the removal of samples from the ground, which minimizes sample disturbance, mitigates volatile losses associated with sample handling, processing and transportation, and removes the need for complex sample extraction and processing equipment. Instead, the analysing instrument is brought to the sample as an integral part of the iDRILL instrument.
The iDRILL functional principle is based on a hollow augered drill shell that can be drilled into lunar regolith. The drill shell encloses a sample volume of 109 cm³ for 10 cm insertion depth, equivalent to 163 – 185 g sample mass, depending on local densities).

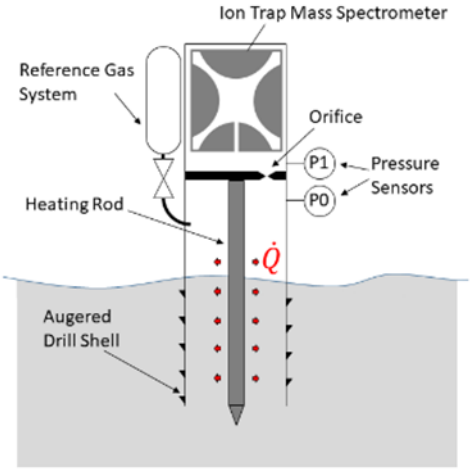

Figure 1: Schematic of IDRILL measurement principle

The baseline length of the drill shell is 12 cm but can be scaled and adapted to the mission needs and boundary conditions. Inside the drill shell a central heating rod is located, which allows outgassing of the sample. The majority of the released gases is trapped inside the drill shell above the regolith surface, but a small amount is able to escape through the lower open end. Pirani pressure sensors monitor the increase in pressure inside the shell, which provides an indication of the volatiles abundance in the sample. An Ion trap mass spectrometer for the analysis of the released volatiles is attached to the sample volume by an orifice. The orifice controls the gas flow from the sample to the mass spectrometer to ensure acceptable gas pressures and is an important design parameter that can be tailored to expected volatiles contents. A reference gas system consisting of a small pressurized gas vessel and a piezo actuated valve allow for in-situ recalibration of the instrument to deal with potential cross-contamination. shows a schematic of the working principle. The PDR design is shown in .

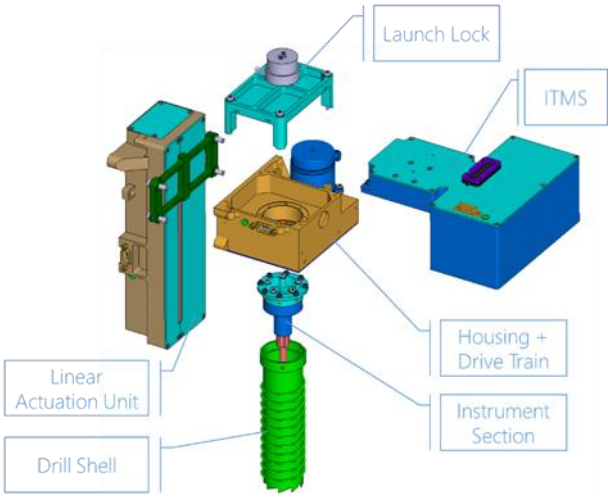

Figure 2: IDRILL PDR Design

2 SCIENCE CASE

The possible existence of water and other volatiles on the Moon - key resources for future, sustainable lunar and interplanetary exploration - and their possible applications has been a topic of intense discussion among scientists, ever since it was first proposed [1]. The issue has been studied intensively in the last two decades and a fleet of remote observation missions, using a variety of instruments, have yielded an increasing amount of evidence for the existence of water ice on the Moon. Bi-static radar observations indicate near-surface water ice in Permanently Shadowed Regions (PSR) [2] and neutron spectroscopy data from multiple instruments indicates elevated hydrogen abundances at higher latitudes and inside large PSRs ([3]; [4]). Near infrared spectroscopy results indicate diurnal changes in surface hydration and general increased surface hydration towards higher latitudes ([5]; [6]). There are also indications of exposed surface ice inside PSRs from infrared, UV and laser reflectance measurements ([7]; [8]). Near Infrared and UV emissions indicated a total water content of 5.6 +/- 2.9%wt in the ejecta plume of Cabeus crater. Elsewhere on the Moon, sensitive orbital mineralogical mapping has revealed the widespread prevalence of OH phases in the topmost layer of the regolith that are hypothesized to be forming under the influence of the solar wind, with abundance fluctuations driven by diurnal cycles ([5], [10]). Despite this plethora of data, interpretations on the amount and nature of volatiles on the surface remain inconclusive and sometimes ambiguous ([11]). Therefore, ground truth data is essential for determining the true nature and abundance of volatiles on the lunar surface.

Expected volatiles abundance

Near infrared reflectance measurements from the Moon Mineralogy Mapper (M3) on Chandrayaan-1 and others suggest OH-enrichment of the top layer of the lunar surface. Based on this data, [6] theorize surface OH/H_2O contents at higher latitude to be as high as ~500 to 750 ppm. Hydration at lower latitudes is generally lower but can be locally enriched at specific surface features like pyroclastic deposits. Diurnal variations of the inferred water contents of up to 200 ppm have been observed, suggesting a strong dependence on illumination and local surface temperatures (see Figure 3). Observations from Lunar Prospector Neutron Spectrometer (LPNS) [12] and Lunar Energetic Neutron Detector (LEND) [4] show increased hydrogen abundances towards higher latitudes. Water-equivalent-Hydrogen (WEH) abundances are estimated at up to 500 ppm in the general polar area [13]. Volatiles abundances are expected to be significantly higher in PSRs, with specific interpretations of NS data with higher spatial resolutions estimating WEH abundances between 0.2-3 wt% [14]. This is also consistent with NIR, UV and Radar observations ([7]; [8]; [2]) that indicate exposed water ice in PSRs and the LCROSS impact measurement [9]. Furthermore, model predictions suggest that water-rich cold traps lose a certain amount of volatiles to their immediate surroundings due to impact vaporization and solar wind sputtering. This would mean that increased concentrations (>750 ppm) of volatiles may be found in the more easily accessible vicinity (like the rims of the craters) of major PSRs.

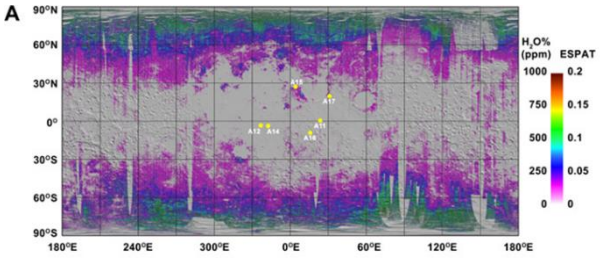

Figure 3: Inferred global water content from M3 NIR measurements [6]

Necessary extraction temperature

Cold trapped volatiles can be released from regolith at relatively low temperatures. Water ice sublimation in vacuum is <1kg/m² for temperatures below 110 K but increases steeply with temperature [15]. Persistence times of water ice become negligible at temperatures above 250 K. Water may also be surface adsorbed (physiosorbed) or chemisorbed, which would require higher release temperatures. Reference [16] determined that physiosorbed H_2O desorbs around 120-150 K, chemisorbed H_2O, OH and H around 180 K and strong chemisorbed water at 400 K. Early studies [17] also showed that significant amounts of volatiles could be extracted from Apollo 16 samples in this temperature range.

Strongly chemisorbed water has a persistence time of ~100 s at a temperature of 400 K, allowing release in a matter of minutes [18].

Outside of polar cold traps, the majority of volatiles likely originated from solar wind, so called solar wind implanted particles (SWIPs), [22] predicted that up to 80% can be extracted by heating the sample to 600°C (873 K) and almost all by heating above 900°C (1173 K).

Necessary drilling depth:

Volatiles in cold-traps depend on local temperatures remaining stable. For example, water ice remains stable for geologic time scales if kept below 110 K [15]. Without a tempering atmosphere, lunar surface temperatures are strongly dependent on solar irradiance. The lunar polar areas feature about 29000 km² of PSRs [19], most of which have maximum annual surface temperatures far below 100 K (see Figure 4). While this raises the possibility of surface water ice in PSRs, they are typically located in rough terrain and inherently difficult to access for solar powered landers or rovers.
Persistent temperatures below 110 K can also be found in the lunar subsurface, covered by a thin layer of regolith. Model predictions from [20] based on DIVINER measurements showed subsurface ice stability is possible at a significant portion of the lunar south polar area.

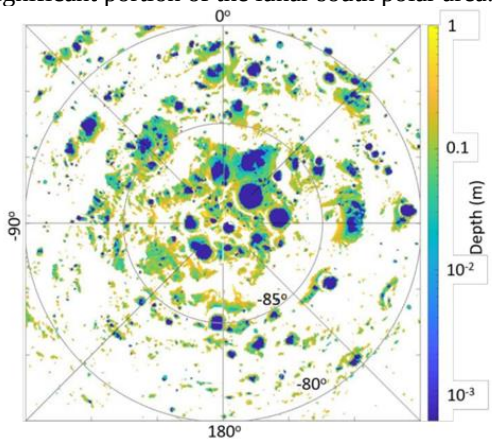

Figure 4: Water ice stability depth at the lunar south pole predicted by the O3DTH [29]

While a drill depth of up to 1 m is beneficial, large areas exist where ice is stable at depths less than 10 cm, being well within the capability of the LVS instrument as pre-developed by our team. More recent studies (e.g. [28]) come to similar results with models featuring significantly increased spatial resolution or more precise material parameters, which is shown in Figure 4. However, ice stability appears to be negatively correlated with surface illumination [14], which provides a challenge for solar powered missions.
No in-situ confirmation of subsurface water ice exists to date, but orbital exosphere measurements from the Neutral Mass Spectrometer on the LADEE spacecraft have shown regular water releases consistent with the impact of meteorite showers on hydrated soil (220 – 520 ppm) covered by a desiccated regolith layer (8 cm) [21].

3 iDRILL DESIGN DESCRIPTION

The iDRILL instrument consists of four subsystems. The linear actuation unit (LAU), the probe head including the drill mechanics and the instrument section, an ion-trap mass spectrometer, and electronics.

Linear Actuation Unit

The Linear Actuation Unit (LAU) is a 1-DOF mechanism, required to raise and lower the Probe Head. It provides two main operational modes to support and enable the drilling operations. The first mode is a constant velocity mode: the iDRILL is lowered from its storage position in either a rover or lander until the tip of the drill is in contact with the lunar surface. Once the rotational motion of the drill shell starts, the LAU lowers the iDRILL into the lunar regolith with constant speed, while directly monitoring the axial loads using a force sensor in order to provide shut-off information in case the axial load exceeds a certain threshold. The second mode is a constant axial force mode: here, during the drilling operation, the LAU controls the axial movement to provide constant axial loads on the drill, again by using information from the inbuilt force sensor. The linear vertical movement is enabled through a combination of self-locking spindle and linear guiding, actuated by a brushed DC actuator.

Probe Head

The Probe Head contains all sub-units required for the scientific measurements:
- Drill Shell & Heater
- Drill Drive Train
- Orifice & Pressure Sensors
- Ion-Trap Mass Spectrometer
- In-Situ Gas Calibration System

The drill shell has an inner diameter of 38 mm, a wall thickness of 1 mm and is augered on the outside. The bottom end features a special cutting edge geometry (see Figure 5), which was optimized in various experiments. To withstand the high temperatures in the vicinity of the heater and for mechanical stability, it is machined from a titanium alloy. The length of the shell can be adjusted to the specific needs of each mission in order to satisfy the individual envelope and drill-depth requirements.

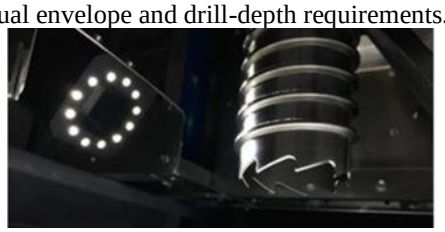

Figure 5: Drill Shell Cutting Edge Geometry

The drill is actuated using a brushless EC pancake actuator through a combination of planetary and spur gears. It is supported at one end through two pre-loaded ball bearings which provide sufficient support to omit

additional support of the drill during launch and descent. A ceramic heating rod is located inside the drill shell. It is based on a commercial heating element, which uses a ceramic tube with imprinted resistor paths. The tube is embedded in a ceramic insulator element. The heating rod is hollow, which allows the insertion of 2 thermocouples to monitor the temperature. With a heating power of 15 W, maximum temperatures of up to 700°C can be reached. Analysis has shown that for 90 min of heating with 15 W, a majority of the sample volume exceeds 400 K. A smaller proportion of the sample exceeds 873 K, thus iDRILL is also able to release Solar Wind Implanted Particles. In practice, both heating power and duration need to be tailored to the specific mission profile.

The orifice, which is located in the probe head above the drill shell, allows released volatiles to travel from the sample volume to the mass spectrometer. It consists of thin copper foil, with a hole of known diameter, held in place by a clamping flange. The orifice foil can be exchanged in the design to adapt to different expected soil volatiles contents. The most important function of the orifice is to regulate the pressure between the drill shell and the mass spectrometer. The mass spectrometer can only safely function at low pressures, whereas pressures inside the drill shell can exceed 10 mbar, depending on the volatiles content of the soil. Therefore, careful selection of the orifice diameter ensures that the mass spectrometer will stay within its pressure range.

The pressure sensors in the instrument section are MEMS Type Pirani Vacuum Sensors. They are used to measure the gas pressure of released volatiles in the volume enclosed by the drill shell above the regolith. Furthermore, they monitor the pressure drop over the orifice. A wheatstone bridge circuit is used to read the sensors.

Ion-Trap Mass Spectrometer

The Ion Trap Mass Spectrometer has been developed under responsibility of The Open University and is based on the Ptolemy flight-proven instrument. This device offers a mechanically simple, low mass, volumetrically compact instrument that can be used to perform rapid identification and characterisation of volatiles in real time as they are liberated from the lunar regolith. The ion trap mass spectrometer consists of a number of discrete subsections: ion source, detector, and an in-situ calibration unit.

The ion source consists of a conventional electron source which ionises the sample gas via electron bombardment. The mass selector is formed from three hyperbolic electrodes that form an electro-potential region within their structure. By manipulation of the amplitude and/or frequency of the potential on the hyperbolic electrodes, ions can be trapped or manipulated to eject them in order of their mass-to-charge ratio.

The detector, which consists of an electron multiplier that detects individual ions as they leave the mass selector, and through a process of amplification, multiplies this extremely low current associated with single ions into signals that can be measured by the control electronics.

Finally, a provision for in-situ calibration of the instrument is provided through the use of a miniaturised calibration gas storage and delivery system. Recent developments in valve technology at The Open University will be employed to provide a reference gas storage system that allows extremely precise flows of gas to be delivered to the instrument to allow in situ calibration during operation, thus increasing the scientific return of the instrument with regards to characterising the liberated volatiles over an extended time period. The new valve technology offers an extremely low leak rate with extremely fast actuation times and low power requirements. The composition of the reference will be selected to give a number of known m/z peaks across the operating range of the instrument.

Control Electronics

The iDRILL also has individual Control Electronics (also referred to as backend electronics) which are interconnected to the different sub-units by an internal harness. The “backend” Control Electronics hosts the majority of electronics. Only the electronic functions which need to be close to the mass spectrometer or actuator elements without a harness in between will be placed in the front end. They will be able to be exposed to a harsher environment while the majority of complex electronics remains protected within its platform bay. The electronics was defined and elaborated on specification level based on an analysis of the lifecycle and a functional analysis to satisfy the needs within a given environment over its lifetime. A dedicated control module will interact with the platform TM/TC interface and steer the internal interfaces to interact with the spectrometer tube, the drill and mechanism drives as well as the heater element.

iDRILL Key Characteristics

Key resource characteristics of the iDRILL instrument are summarized in Table 1.

Table 1: iDRILL Key resource characteristics

Instrument front-end envelope (L x W x H, 12 cm drill shell)	162 x 241 x 284 mm³	
Instrument Mass	Instrument (incl. LAU)	4650 g
	Back-End Electr.	2160 g
	Int. Harness (0.5 m)	190 g
Instrument Required Power	Drilling Mode	30 W
	Heating & Evolved Gas Analysis Mode	15 W
Instrument Mechanical Interface	TBD (adaptable to mission)	
Minimum Survival Temperature (without additional integr. heaters)		-60 °C

4 FUNCTIONAL AND PERFORMANCE TESTING

Currently, the consortium has designed and built test setups for vacuum and mechanical testing, which enable the experimental verification of the instrument [30]. The mechanical testing set up allows the simultaneous measurement of both force and torque during insertion. The lunar environment was simulated with the lunar regolith simulant JSC-1A. Three sets of samples were tested: dry and wet (2.5% & 5% hydration). In addition, the wet samples were frozen up to -35° and also tested with the drill. Also, a test campaign utilizing wet sand was conducted (see impression in Figure 6).

Figure 6: iDRILL testing in wet sand.

Penetration Torque and Force

Penetration torque and force are important parameters as they represent the exported loads of the iDRILL instrument during operation and need to be counteracted by the carrying vehicle. The iDRILL instrument can determine the loads and adjust its operations to stay below certain thresholds. To determine the magnitude of the instrument, penetration force and torque measurement were performed using the iDRILL breadboard in a laboratory environment (1 g, 1 atm). Measurements were performed in a defined and mechanically representative way by attaching the available breadboard to a linear drive mechanism including torque meter and load cell. The tests were conducted using JSC-1A lunar regolith simulant and the testbed was prepared using rake and shovel following a technique also used for the preparation of the ExoMars testbeds [23]. Tests were performed using *dry* and *wet* soil samples. For the *wet* tests, a mixture of JSC-1% with 2.5% and 5% water content was prepared and frozen using liquid nitrogen. The averaged results are presented in Figure 7. It can be seen that the penetration force rises nearly linearly during the first 10 cm or insertion and rises significantly for deeper depth. During the 0% humidity tests the penetration force is slightly larger than during the tests with wet soil. The hypothesis is that this is due to water ice melting when in contact with the rotating drill shell, thus creating a lubricating layer during the drilling operation. This would not be possible in a lunar environment as the water would sublimate instead of melting. This will be taken into consideration and especially investigated in future thermal vacuum tests.

As mentioned above, penetration force and torque are key figures and important control parameters in order to not exceed mission specific thresholds. Both parameters can be influenced by adjusting the speed ratio of drill and linear actuation. A speed ratio of 1, meaning that the augered drill shell is threaded into the soil, a speed ratio > 1 means that the drill rotates faster with respect to the linear feed. The penetration resistance generally increases with soil bulk density, but a higher ratio of rotational speed to vertical downward motion can decrease resistance.

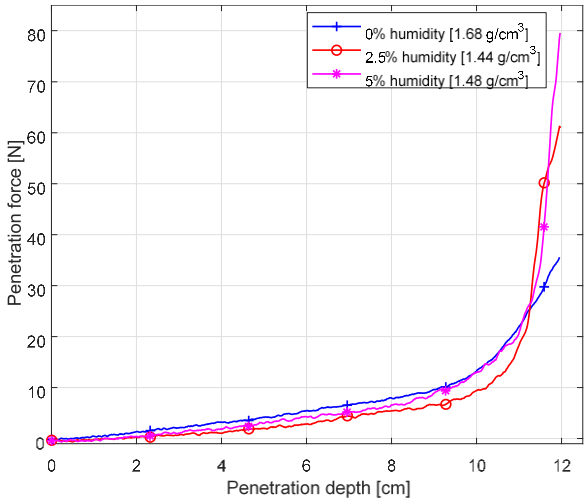

Figure 7: Average penetration forces for JSC-1A with different water contents for a speed ratio SR = 1

This is shown in Figure 8 where the penetration resistances for different rotational speeds is shown in highly compacted regolith. Increased rotational speeds also increase soil disturbance, so a lower rotational velocity is preferable wherever possible. Results show that a speed ratio of 2 (twice as many rotations as a screw in a thread) yields a penetration resistance of up to 10 N for a depth of 10 cm in loose regolith, but a speed ratio of 10 would yield a similar force in highly compacted regolith.

The shape of the penetration resistance over depth is typically mostly linear for the first centimetres and then takes an exponential shape. The reasons for this are, that bulk density generally increases with depth and the shear resistance of a plane of regolith depends on the pressure acting on that plane, which also increases with depth by the weight of the soil above. However, this pressure also depends on the gravitational constant, therefore actual resistances on the lunar surface should be considerably smaller. In any case, the iDRILL instrument can easily penetrate up to a depth of 12 cm, depths up to 20 cm should be possible if the regolith is not too dense. If problems are encountered, high speed ratios can help to lower the resistance but potentially increase the time

required for drilling.

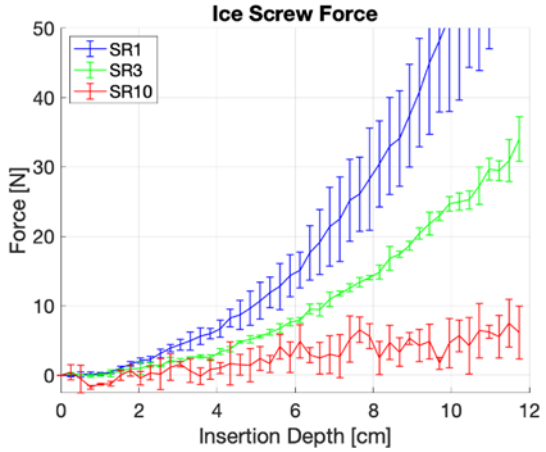

Figure 8: Vertical insertion force with the baseline drill geometry and different speed ratios (SR = speed ratio). Error bars show standard deviation (1σ). Regolith density approx. 1.9 g/cm³

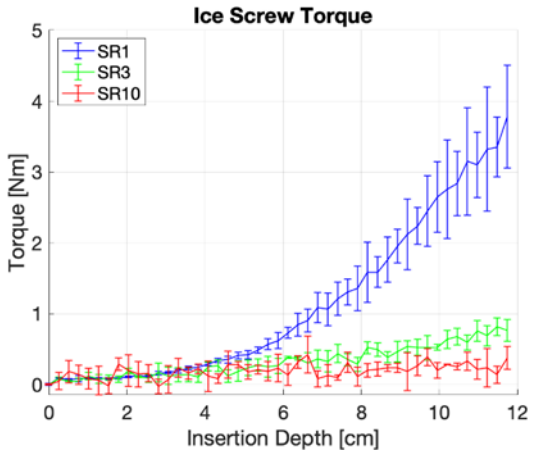

Figure 9: Required drill torque (right) for the LVS with the baseline drill geometry and different speed ratios (SR = speed ratio). Error bars show standard deviation (1σ). Regolith density approx. 1.9 g/cm³

The effects on the drilling torque are similar to the one for the penetration force and presented in Figure 9. For lightweight carrying vehicles or high density regolith, a larger speed ratio will be beneficial to keep the exported torques sufficiently low.

Cross-Contamination

For iDRILL, two different means of cross contamination need to be taken into account. The transfer of granular material from one sampling site to the following ones, and the transfer of volatiles.

The aspect of granular cross-contamination has already been addressed under the original LUVMI development of the Lunar Volatiles Scout (LVS). After a performed drilling, it cannot be avoided that soil adheres to the inside of the shell. Thus, during the following drilling operation, the new sample is contaminated with the residual material from previous operations. The amount of this cross-contamination was tested using the LVS prototype and lunar regolith simulant (JSC 1A). It could be shown that, on average, 0.026 g of regolith adhered to the inside of the drill shell as long as the shell was rotated upon extraction. Static extraction – i.e., not running the drill drive – increased the amount of cross-contamination by 26% to an average of 0.035 g [24]. Figure 10 shows microscopic images of the inner shell surface after drilling operations.

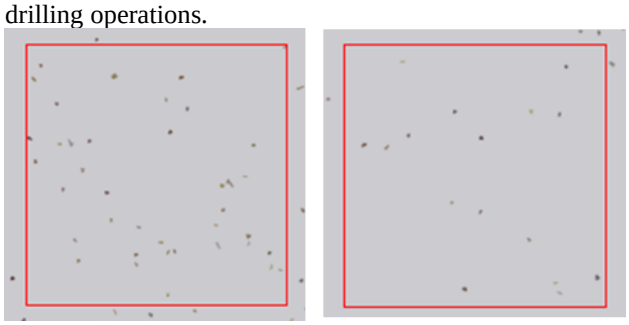

Figure 10: Microscope captures at 50x magnification of the shell internal surface samples taken right after drilling operation (left: static extraction; right: dynamic extraction)

The assessment shows that the prototype design very likely is uncritical in terms of cross-contamination as the amount of soil enclosed by the shell during heating and volatile extraction exceeds the amount of residual materials by orders of magnitude.

Furthermore, the impact of cross contamination on the samples can be even further reduced by heating the extracted drill. This would potentially allow to increase the temperature of the drill shell and all particles still adhering to it, releasing all volatiles potentially still bound to those grains or adhering to other parts of the drill. Those volatiles could then escape through the open end of the drill. The transport volatiles from one sampling site to another could therefore be even further reduced. This approach is baselined for lunar operations.

A special case with respect to cross contamination would be large pebbles getting stuck between heater and drill shell significantly increasing the amount of sample material kept in the drill. Tests were carried out to assess the criticality of this scenario as well as to identify procedures to remove such stuck samples. The results are presented below.

Pebble Testing

Lunar regolith can be described as a pebble/cobble bearing soil [25], with a wide particle size distribution and a non-negligible number of larger rocks. This is relevant to the iDRILL development, because rocks could a) prevent successful insertion, b) damage the drill shell or heating rod and c) get stuck between heating rod and drill shell.

If the iDRILL instrument hits a rock during insertion, it

is possible that the available downward force and torque are insufficient for the drill to penetrate. The iDRILL drill is designed for granular material, not solid rock. The likelihood of unsuccessful penetration increases with the size of the pebble. However, this scenario is not critical, as the insertion attempt can simply be stopped and repeated elsewhere.

The drill shell has an inner diameter of 38 mm, the heating rod a diameter of 8 mm. It is therefore possible that pebbles with dimensions 10 – 15 mm enter the drill shell and could get stuck, in the worst case. While it is beneficial that the drill shell rotates against the static heating rod, thus introducing a relative motion between these elements, the possibility of a pebble getting stuck remains.

To get an idea of the magnitude of the risks posed by the above scenarios, the following provided an estimate of the amount of pebbles in relevant sizes that are to be expected. During the Apollo 15, 16 and 17 missions, the Astronauts conducted a total of 24 raking sample acquisitions. Values obtained [26] based on video footage were used to estimate the total soil volume that was probed to about 1.3 m^3. In this volume, a total of 665 rocks were gathered [27]. Therefore, there are on average: 5.1 x 10^{-4} rocks/cm^3 (rocks = rocks / cobbles / pebbles > 1 cm).

For each sampling, the iDRILL encloses or displaces up to 189 cm^3 of regolith (for an insertion depth of 15 cm), therefore the chance of hitting a pebble of relevant size is 9.7% for each drilling operation. Over a total of 50 samplings, the probability of hitting at least one rock is >99% and the expected number of rocks hit is: 4.8 rocks/(50 samples) .This shows that it is unavoidable to hit at least one rock over the iDRILL lifecycle.

Damage to the iDRILL is possible, therefore a hazard mitigation strategy is necessary. It is envisaged to use the force sensor to detect anomalous insertions to potentially abort drilling when a rock is hit.

With a probability of hitting a rock less than 10% per sampling, aborting a drilling operation will not put an unreasonable strain on the overall mission.

The impact of pebbles on the drilling was investigated experimentally, with a focus on the possibility of pebbles getting stuck in the drill shell.

These experiments have been carried out with especially prepared samples to provoke pebbles entering the cavity between drill shell and heating rod during drilling operation. These experiments have shown that

~35% of pebbles get pushed into shell

~50% get stuck (17.5% total)

100% of stuck pebbles were released by rotation

For a total instrument lifetime of ~50 samples and with a chance of hitting pebbles of 9.7% per sampling operation:

5 pebbles will be encountered

2 pebbles will be pushed into shell

1 pebble will get stuck

Figure 11 shows examples of the situation after the test prior to the start of the recovery procedure. The operational recovery procedure foresees a counter-rotation during extraction of the drill shell (not performed in these tests). This will facilitate the removal of pebbles during extraction. Based on the results of these tests, it is recommended to add a further rotation / counter-rotation step once the shell is fully extracted.

Figure 11: Examples of pebbles after testing

There is a residual risk that a pebble will remain stuck (especially under lunar gravity). However this is not a total mission loss, iDRILL could still operate (with higher cross-contamination).

The worst case is damage to the heating rod. This should be tested extensively with a final heater prototype and with actual loads from mission (loads will likely be limited).

Preliminary scratching analysis has nevertheless returned promising results on the mechanical robustness to sharp and hard edges.

Vibration Testing

Sine and Random vibration testing has been carried out to ESA specified levels in order to test the most critical components of the iDRILL instrument: Ion-Trap Mass Spectrometer, ceramic heating rod, and pressure sensors. All tests were successful and all specimens survived without damage.

5 CONCLUSION

The iDRILL design is fully compliant to the preliminary mission requirements established in the frame of the ESA funded iDRILL activity. The design is based on an extensively tested breadboard on the one hand, and significant heritage with exploration mechanisms and instruments on the other hand. It was shown that all required functions can be provided and that the performance is sufficient to satisfy the requirements. After the analysis of different mission scenarios and associated risks, the consortium is confident that the iDRILL design can be accommodated in a short time to the majority of potential flight opportunities which might arise in the near future. It is worth noting that the instrument was designed without having yet selected a specific mission. Required regions of flexibility were identified (e.g. mechanical and electrical interfaces, drilling depth, modular approach, sensors) to be able to adapt the instrument design to any mission scenario with as little impact on cost and schedule as possible.

6 ACKNOWLEDGEMENTS

This development activity took place through the European Commission's Horizon 2020 program, with a design evolution through the LUVMI and LUVMI-X grants (grant numbers 727220 & 822018). In the frame of the recent iDRILL project, funded by the European Space Agency under contract 4000132715/20/NL/AT, the design of critical elements was advanced to PDR level and TRL 5.

The iDRILL consortium would like to thank ESA Technical Office and the PDR reviewer panel for the great collaboration, valuable feedback, and the enthusiasm in advancing such an incredibly interesting development.

7 REFERENCES

1. Watson, K.; Murray, B. C.; Brown, H. (1961): On the possible presence of ice on the Moon. In: J. Geophys. Res. (66), S. 1598–1600.
2. Nozette, S.; Lichtenberg, C. L.; Spudis, P.; Bonner, R.; Ort, W.; Malaret, E. et al. (1996): The Clementine bistatic radar experiment. In: Science 274 (5292), S. 1495–1498. DOI: 10.1126/science.274.5292.1495.
3. Elphic, R. C.; Eke, V. R.; Teodoro, L. F. A.; Lawrence, D. J.; Bussey, D. B. J. (2007): Models of the distribution and abundance of hydrogen at the lunar south pole. In: Geophys. Res. Lett. 34 (13), n/a-n/a. DOI: 10.1029/2007GL029954.
4. Mitrofanov, I.; Litvak, M.; Sanin, A.; Malakhov, A.; Golovin, D.; Boynton, W. et al. (2012): Testing polar spots of water-rich permafrost on the Moon: LEND observations onboard LRO. In: J. Geophys. Res. 117 (E12), n/a-n/a. DOI: 10.1029/2011JE003956.
5. Pieters, C. M.; Goswami, J. N.; Clark, R. N.; Annadurai, M.; Boardman, J.; Buratti, B. et al. (2009): Character and Spatial Distribution of OH/H2O on the Surface of the Moon Seen by M3 on Chandrayaan-1. In: Science 326 (5952), S. 568–572. DOI: 10.1126/science.1178658.
6. Li, Shuai; Milliken, Ralph E. (2017): Water on the surface of the Moon as seen by the Moon Mineralogy Mapper: Distribution, abundance, and origins. In: Science Advances 3 (9). DOI: 10.1126/sciadv.1701471.
7. Hayne, Paul O.; Hendrix, Amanda; Sefton-Nash, Elliot; Siegler, Matthew A.; Lucey, Paul G.; Retherford, Kurt D. et al. (2015): Evidence for exposed water ice in the Moon's south polar regions from Lunar Reconnaissance Orbiter ultraviolet albedo and temperature measurements. In: Icarus 255, S. 58–69. DOI: 10.1016/j.icarus.2015.03.032.
8. Li, Shuai; Lucey, Paul G.; Milliken, Ralph E.; Hayne, Paul O.; Fisher, Elizabeth; Williams, Jean-Pierre et al. (2018): Direct evidence of surface exposed water ice in the lunar polar regions. In: Proceedings of the National Academy of Sciences 115 (36), S. 8907–8912. DOI: 10.1073/pnas.1802345115.
9. Colaprete, Anthony; Schultz, Peter; Heldmann, Jennifer; Wooden, Diane; Shirley, Mark; Ennico, Kimberly et al. (2010): Detection of Water in the LCROSS Ejecta Plume. In: Science 330 (6003), S. 463–468. DOI: 10.1126/science.1186986.
10. Jones, Brant M.; Aleksandrov, Alex; Hibbitts, K.; Dyar, M. D.; Orlando, Thomas M. (2018): Solar Wind-Induced Water Cycle on the Moon. In: Geophys. Res. Lett. 45 (20), S. 29. DOI: 10.1029/2018GL080008.
11. Teodoro, L. F. A.; Eke, V. R.; Elphic, R. C.; Feldman, W. C.; Lawrence, D. J. (2014): How well do we know the polar hydrogen distribution on the Moon? In: J. Geophys. Res. Planets 119 (3), S. 574–593. DOI: 10.1002/2013JE004421.
12. Feldman, W. C.; Maurice, S.; Lawrence, D. J.; Little, R. C.; Lawson, S. L.; Gasnault, O. et al.: Evidence for water ice near the lunar poles.
13. Sanin, A. B.; Mitrofanov, I. G.; Litvak, M. L.; Bakhtin, B. N.; Bodnarik, J. G.; Boynton, W. V. et al. (2017): Hydrogen distribution in the lunar polar regions. In: Icarus 283, S. 20–30. DOI: 10.1016/j.icarus.2016.06.002.
14. Flahaut, J.; Carpenter, J.; Williams, J.-P.; Anand, M.; Crawford, I. A.; van Westrenen, W. et al. (2020): Regions of interest (ROI) for future exploration missions to the lunar South Pole. In: Planetary and Space Science 180, S. 104750. DOI: 10.1016/j.pss.2019.104750.
15. Feistel, Rainer; Wagner, Wolfgang (2007): Sublimation pressure and sublimation enthalpy of H2O ice Ih between 0 and 273.16K. In: Geochimica et Cosmochimica Acta 71 (1), S. 36–45. DOI: 10.1016/j.gca.2006.08.034.
16. Hibbitts, C. A.; Grieves, G. A.; Poston, M. J.; Dyar, M. D.; Alexandrov, A. B.; Johnson, M. A.; Orlando, T. M. (2011): Thermal stability of water and hydroxyl on the surface of the Moon from temperature-programmed desorption measurements of lunar analog materials. In: Icarus 213 (1), S. 64–72. DOI: 10.1016/j.icarus.2011.02.015.
17. Gibson, E. K.; Moore, G. W. (1972): Inorganic gas release and thermal analysis study of Apollo 14 and 15 soils. In: Proceedings of the third Lunar Science Conference, S. 2029–2040.
18. Reiss, P. (2018): A combined model of heat and mass transfer for the in situ extraction of volatile water from lunar regolith. In: Icarus 306, S. 1–15. DOI: 10.1016/j.icarus.2018.01.020.
19. Mazarico, E.; Neumann, G. A.; Smith, D. E.; Zuber, M. T.; Torrence, M. H. (2011): Illumination conditions of the lunar polar regions using LOLA topography. In: Icarus 211 (2), S. 1066–1081. DOI: 10.1016/j.icarus.2010.10.030.
20. Paige, David A.; Hayne, Paul O.; Greenhagen, Benjamin T.; Foote, Marc C.; Siegler, Matthew A.; Vasavada, Ashwin R. (2010): Diviner Lunar Radiometer observations of the LCROSS impact. In: Science (New York, N.Y.) 330 (6003), S. 477–479. DOI: 10.1126/science.1197135.
21. Benna, M.; Hurley, D. M.; Stubbs, T. J.; Mahaffy, P. R.; Elphic, R. C. (2019): Lunar soil hydration constrained by exospheric water liberated by meteoroid impacts. In: Nature geoscience 12 (May), S. 333–338. DOI: 10.1038/s41561-019-0345-3.
22. L.A. Taylor, W.D. Carrier III, J.S. Lewis, M.S. Matthews, M.L. Guerrieri (Eds.): Oxygen production on the Moon: an overview and evaluation. In: Resources of Near-Earth Space, University of Arizona Press (1993), pp. 69-108
23. Apfelbeck M., Kuß S., Rebele B., and Schäfer B., "A systematic approach to reliably characterize soils based on Bevameter testing," Journal of Terramechanics, vol. 48, no. 5, pp. 360–371, 2011.
24. Reganaz M., "Detailed Design, Assembly, Integration, Test and Contamination assessment for the LUVMI Instrument", Master Thesis, Technische Universität München, Lehrstuhl für Raumfahrttechnik, Prof. Prof. h.c. Dr. Dr. h.c. U. Walter, RT-MA 2018/08, 2018.
25. G. H. Heiken; D. T. Vaniman; B. M. French (Eds.) (1991): Lunar sourcebook : a user's guide to the Moon. Lunar and Planetary Institute: Cambridge University Press.
26. Warren, P.: Lunar Digability Compendium. University of California Los Angeles. Available online at ttp://cosmochemists.igpp.ucla.edu/digability.html, checked on 11/25/2020.
27. Allton, J. H.; Bevill, T. J. (2003): Curatorial Statistics on Apollo Regolith Fragements Applicable to Sample Collection by Ranking. In Advances in Space Research. Available online at https://doi.org/10.1016/S0273-1177(03)00538-6.
28. Reiss, P., Warren, T., Sefton-Nash, E., & Trautner, R. (2021). Dynamics of subsurface migration of water on the Moon. Journal of Geophysical Research: Planets, 126, e2020JE006742. https://doi.org/10.1029/2020JE006742
29. Warren, T. and Bowles, N. and Sefton-Nash, E. and Fisackerly, R. and Trautner, R. (2020): The Oxfod 3D Thermophysical Model with Application to the Lunar PROSPECT Mission. European Lunar Symposium, 152-153, https://els2020.arc.nasa.gov/abstracts
30. Biswas, J.; Sheridan, S.; Pitcher, C.; Richter, L.; Reganaz, M.; Barber, S. J.; Reiss, P. (2020): Searching for potential ice-rich mining sites on the Moon with the Lunar Volatiles Scout. In: Planetary and Space Science 181, S. 104826. DOI: 10.1016/j.pss.2019.104826.